INTERNATIONAL JOURNAL FOR NUMERICAL METHODS IN FLUIDS, VOL. 23, 847–858 (1996)

NATURAL FORMULATION OF THE RANDOM CHOICE METHOD FOR TWO-DIMENSIONAL INERT HIGH-SPEED FLOW FIELDS

A. S. DAWES*

College of Aeronautics, Cranfield University, Cranfield, Bedford, U.K.

SUMMARY

The random choice method has now been shown to be successfully extendible from the original one-dimensional unsteady formulation to inert high-speed flow fields which are steady and two-dimensional using Cartesian, axisymmetric and Lagrangian formulations. This paper deals with the description of a new implementation of the random choice method formulated for natural co-ordinates based on streamlines and normals. Comparisons between theoretical and computed results for several different physical configurations are presented.

KEY WORDS: Euler equations; hyperbolic; initial boundary value problem; natural co-ordinate system; random choice method; Riemann problem

1. INTRODUCTION

The random choice method (RCM) is based on an existence proof by Glimm[1] for solutions to systems of non-linear hyperbolic, one-dimensional, unsteady equations. Chorin[2] developed it into a practical numerical method which was subsequently improved by Colella,[3] Gottlieb,[4] Sod[5] and Toro[6] to name but a few. The equations for steady, two-dimensional, supersonic flow fields are hyperbolic and are similar to the one-dimensional equations. This property has been used to develop the RCM for Cartesian and axisymmetric co-ordinate systems[7–10] and for the Lagrangian co-ordinate system.[11] In recent years the RCM has lost favour to other numerical schemes, for example schemes that incorporate the total variational diminishing (TVD) method.[12,13] This is because the RCM cannot be successfully applied to multidimensional problems.[14] However, there are two strong reasons for using the method which others struggle to match. Firstly, discontinuities, as shocks or contact surfaces, suffer from no numerical diffusion or oscillations. Secondly, shock waves are predicted with infinite resolution.

The Euler equations are presented for the natural co-ordinate system based on streamlines and normals. This choice of co-ordinate space has the advantage of capturing physical boundaries exactly. The RCM is then described in detail. Finally, a comparison of computed and theoretical results for several configurations is presented.

*Present address, AWE Aldermaston, Reading, RG7 4PR, U.K.

CCC 0271–2091/96/080847–12

Received June 1995
Revised January 1996

2. NATURAL CO-ORDINATE FORMULATION OF THE STEADY STATE EULER EQUATIONS

For regions where the flow field variables are continuous functions of position, the steady state Euler equations for conservation of mass, momentum and energy written in vector form are

$$\nabla \cdot (\rho \mathbf{u}) = 0, \tag{1}$$

$$\nabla \cdot (\rho \mathbf{u}\mathbf{u}) + \nabla p = 0, \tag{2}$$

$$\nabla \cdot (\rho \mathbf{u} h_s) = 0, \tag{3}$$

where ρ is the gas density, p is the gas pressure, $\mathbf{u}$ is the velocity vector, h_s is the total specific enthalpy ($= e + p/\rho + \frac{1}{2}q^2$), q is the magnitude of $\mathbf{u}$ and e is the specific internal energy of the gas, which for an ideal polytropic gas is a function of pressure and density thus,

$$e = \frac{p}{\rho(\gamma - 1)}, \tag{4}$$

where γ is the ratio of specific heat capacities.

The natural co-ordinate system for two-dimensional flow fields consists of streamlines ξ_1 and normal ξ_2 (see Figure 1). A unique transformation exists between this and the Cartesian co-ordinate space (x_1, x_2) which is defined by

$$\mathrm{d}x_k = \sum_{i=1}^{2} \frac{\partial x_k}{\partial \xi_i} \mathrm{d}\xi_i, \quad k = 1, 2. \tag{5a}$$

The metrics are given by

$$\frac{\partial x_1}{\partial \xi_1} = \sigma_1 \cos\theta, \qquad \frac{\partial x_1}{\partial \xi_2} = -\sigma_2 \sin\theta, \qquad \frac{\partial x_2}{\partial \xi_1} = \sigma_1 \sin\theta, \qquad \frac{\partial x_2}{\partial \xi_2} = \sigma_2 \cos\theta, \tag{5b}$$

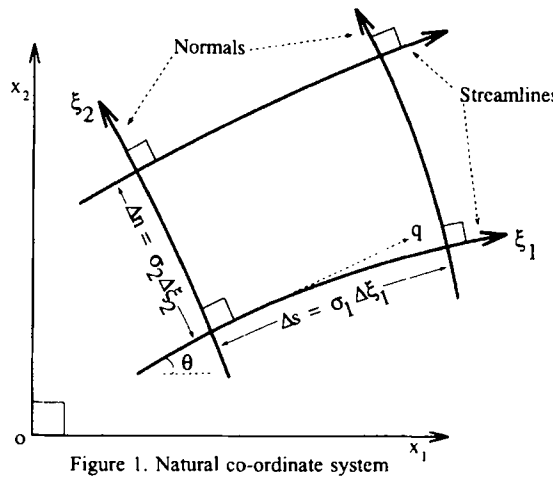

Figure 1. Natural co-ordinate system

where θ is the angle between a tangent to a streamline and a reference direction and σ_1 and σ_2 are scaling factors.[15] Elemental arc lengths measured along the streamlines and normals are defined in terms of the scaling factors and elemental changes in the respective co-ordinates. Thus increments of length s along a streamline and n along a normal are given by

$$\mathrm{d}s = \sigma_1 \mathrm{d}\xi_1, \qquad \mathrm{d}n = \sigma_2 \mathrm{d}\xi_2. \tag{6}$$

Using the above definitions and noting that the velocity vector has only one component, which must be tangential to a streamline, equations (1)–(3) can be written in strong conservation law form[16] for the natural co-ordinate system as

$$\frac{\partial F(U)}{\partial \xi_1} + \frac{\partial G(U)}{\partial \xi_2} = 0, \tag{7a}$$

where

$$F(U) = \begin{pmatrix} \rho q \sigma_2 \\ (\rho q^2 + p)\sigma_2 \cos\theta \\ (\rho q_2 + p)\sigma_2 \sin\theta \\ \rho q \sigma_2 h_s \\ \sigma_2 \cos\theta \\ \sigma_2 \sin\theta \end{pmatrix}, \qquad G(U) = \begin{pmatrix} 0 \\ -p\sigma_1 \sin\theta \\ p\sigma_1 \cos\theta \\ 0 \\ -\sigma_1 \sin\theta \\ \sigma_1 \cos\theta \end{pmatrix} \tag{7b}$$

and $U = (\rho, q, p, \theta, \sigma_1, \sigma_2)^{\mathrm{T}}$. The first four terms of the system (7a) represent conservation of mass, momentum along a streamline and normal, and energy. The last two terms are due to the co-ordinate transformations. The mass and energy terms can be integrated immediately to yield

$$\rho q \sigma_2 = m(\xi_2), \qquad h_s = H_s(\xi_2), \tag{8}$$

where $m(\xi_2)$ and $H_s(\xi_2)$ are the mass per unit length and total enthalpy respectively, with both functions remaining constant along a given streamline.

The system (7a) together with the initial conditions

$$U(\xi_2) = U(0, \xi_2), \qquad \theta_b(\xi_1) = \theta(\xi_1, 0) \tag{9}$$

defines an initial boundary value problem (IBVP). However, it is underdetermined, as σ_1 cannot be calculated downstream from the present conditions. By using (7a),[17] it is seen that this is a consequence of the streamline curvature κ_1 being directly dependent on the pressure gradient normal to a streamline,

$$\kappa_1 = -\frac{1}{\sigma_1}\frac{\partial \theta}{\partial \xi_1} = \frac{1}{\sigma_1 \sigma_2}\frac{\partial \sigma_1}{\partial \xi_2} = \frac{1}{\rho q^2 \sigma_2}\frac{\partial p}{\partial \xi_2}. \tag{10}$$

Therefore, until the variation of the normal pressure gradient is known along ξ_2, the streamline curvature and ultimately σ_1 cannot be determined. The last two terms in equation (10) can be integrated along ξ_2 to yield an expression for σ_1,

$$\ln(\sigma_1) = \int_{\xi_2} \frac{\mathrm{d}p}{\rho q^2}, \tag{11a}$$

together with the boundary condition for closure,

$$\sigma_{1b}(\xi_1) = \sigma_1(\xi_1, \xi_2 = \text{constant}). \tag{11b}$$

For isoenergetic and irrotational flow fields, equation (11a) can be integrated to yield[18]

$$\sigma_1 = \frac{g(\xi_1)}{q}. \tag{11c}$$

For supersonic flows, $M > 1$, the system (7a) is fully hyperbolic with real eigenvalues

$$\lambda_0 = 0 \quad \text{(multiplicity two)}, \qquad \lambda_\pm = \pm \frac{\sigma_1}{\sigma_2} \tan(\mu), \tag{12}$$

where $\lambda = d\xi_2/d\xi_1$, $\mu = \sin^{-1}(1/M)$, $M = q/a$ is the Mach number and $a = (\gamma p/p)^{1/2}$ is the speed of sound. The Riemann invariants, which are independent of the co-ordinate system, have the form

$$\nu(M) \mp \theta = J_\pm, \tag{13}$$

where $\nu(M)$ is the Prandtl–Meyer (PM) function[17,19] and $J_\pm$ are constants for the characteristic directions.

2.1. Discontinuous solutions

For regions where the flow field variables are discontinuous functions of position, the Euler equations are replaced by the Rankine–Hugoniot jump relations.[19] The integral equation for σ_1 must also be replaced by jump relations across the discontinuity. For contact discontinuities,

$$[\sigma_1] = 0, \tag{14}$$

and for oblique shock waves,[18]

$$[\sigma_1 q] = 0, \tag{15}$$

where $[f] = f_2 - f_1$ represents the difference between values across the discontinuity.

3. THE RANDOM CHOICE METHOD

The (ξ_1, ξ_2) co-ordinate space is discretized (see Figure 2) with the ξ_2-co-ordinate divided up, $0 < (\xi_2)_1 < (\xi_2)_2 < \ldots < (\xi_2)_N$, into N equally spaced cells with cell centre and streamline position $(\xi_2)_j$, width $\Delta\xi_2 = (\xi_2)_{j+1} - (\xi_2)_j$ and boundaries $(\xi_2)_{j\pm1/2} = (\xi_2)_j \pm \frac{1}{2}\Delta\xi_2$. A pseudocell is introduced at $j = 0$, where the flow is the mirror image of the flow in the cell $j = 1$, which takes into account the tangential flow at the solid surface $\xi_2 = 0$. For the far-field boundary, taken at $\xi_2 = 1$, another pseudocell is added at $j = N + 1$ with transmissive flow conditions. The ξ_1-co-ordinate is discretized with normal co-ordinate position $(\xi_1)_i$. The incremental step size $\Delta\xi_1 = (\xi_1)_{i+1} - (\xi_1)_i$ is controlled by the Courant–Friedrich–Lewy (CFL) stability criterion.[20] The initial conditions are approximated by a set of piecewise constant states with values remaining constant in each cell, $\bar{U}_{i,j}$, but changing discontinuously at the cell interfaces,

$$\bar{U}(\xi_2) = \begin{cases} \bar{U}_L, & \xi_2 > (\xi_2)_{j+1/2}, \\ \bar{U}_R, & \xi_2 < (\xi_2)_{j+1./2}, \end{cases} \tag{16}$$

where we have used the notation $\bar{U}_L = \bar{U}_{i,j+1}$ and $\bar{U}_R = \bar{U}_{i,j}$. The system (7a) together with the initial conditions $\bar{U}(\xi_2)$ corresponds locally to a Riemann problem denoted by RP$(j, j+1)$.

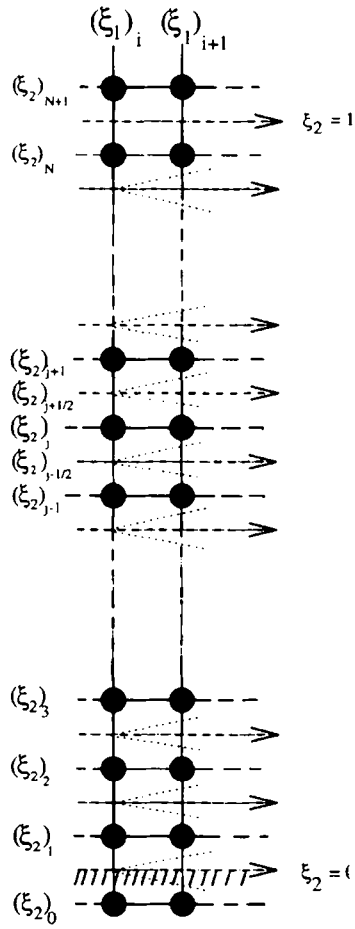

Figure 2. Computational grid

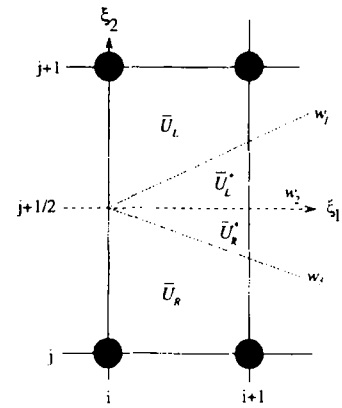

Figure 3. Solution of Riemann problem

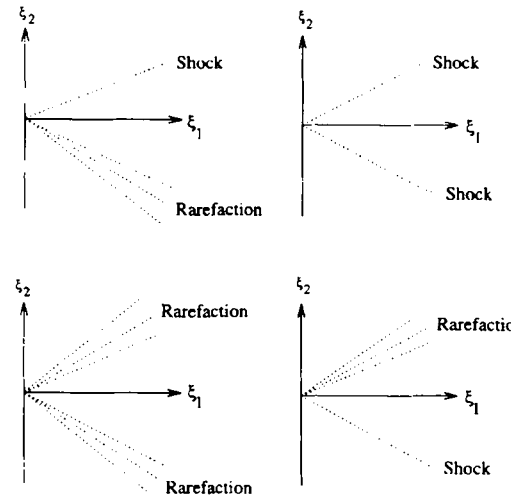

Figure 4. Wave permutations

The solution of an RP is based on the similitude

$$\left(\frac{\xi_2 - (\xi_2)_{j+1/2}}{\xi_1 - (\xi_1)_i}\right)$$

and consists of left- and right-running waves propagating outwards from the initial discontinuity at the cell interface (see Figure 3). The waves w_1 and w_3 can be either an oblique shock wave or a PM rarefaction wave. Four permutations of these waves are possible as represented schematically in Figure 4. They are separated by the contact wave w_2 which is coincident with the streamline direction ξ_1. The two regions downstream of the waves are uniform and will be known as the centred state or *-state. Since the pressure and flow angle are continuous across the contact w_2, the pressure in the centred state p^* (from which all other variables can be calculated) can be written in terms of the left and right states as

$$f(p^*; U_L, U_R) = \theta_L - \theta_R - \chi_L - \chi_R = 0, \tag{17a}$$

where

$$\chi_{L,R} = \begin{cases} [v]_{L,R}, & \eta_{L,R} \leqslant 1, \\ -\tan^{-1}\left(\dfrac{\cot(\beta_{L,R})(\eta_{L,R}-1)}{\gamma M_{L,R}^2 - (\eta_{L,R}-1)}\right), & \eta_{L,R} > 1, \end{cases} \tag{17b}$$

$$\kappa_{L,R} = \begin{cases} (\eta_{L,R})^{1/\gamma}, & \eta_{L,R} \leqslant 1, \\ \dfrac{2\gamma + (\gamma+1)(\eta_{L,R}-1)}{2\gamma + (\gamma-1)(\eta_{L,R}-1)}, & \eta_{L,R} > 1, \end{cases} \tag{17c}$$

$$\cot(\beta_{L,R}) = \sqrt{\left(\frac{2\gamma M_{L,R}^2 - \eta_{L,R}(\gamma+1) - (\gamma-1)}{(\gamma-1) + \eta_{L,R}(\gamma+1)}\right)}, \tag{17d}$$

$$M_{L,R}^* = \sqrt{\left\{\frac{2}{\gamma-1}\left[\frac{\kappa_{L,R}}{\eta_{L,R}}\left(1 + \frac{\gamma-1}{2}M_{L,R}^2\right) - 1\right]\right\}}, \tag{17e}$$

$\chi_{L,R} = \mp [\theta]_{L,R}$, $[\phi]_{L,R} = \phi_{L,R}^* - \phi_{L,R}$, $\beta_{L,R}$ is the oblique shock wave angle in the left and right states, $M_{L,R}^*$ is the Mach number in the left and right centred states, $\kappa_{L,R} = \rho_{L,R}^*/\rho_{L,R}$ is the density ratio and $\eta_{L,R} = p^*/p_{L,R}$ is the pressure ratio. Equation (17a) cannot in general be solved analytically but was solved using Müller's iterative-based method.[10,18,21]

The evolution of the flow downstream at the next spatial position $(\xi_1)_{i+1}$ results from the wave interaction originating at the cell boundaries between adjacent cells at $(\xi_1)_i$. The position of the waves in each RP can be determined once the piecewise constant variation in σ_1 along ξ_2 has been calculated from the boundary value σ_{1b} using either equation (11c) for rarefaction waves or equation (15) for oblique shock waves, together with equation (14) for the contact discontinuity. It should be pointed out that equations (11c) and (15) are equivalent and can be written as $\sigma_1 q = \text{constant}$. For σ_{1b} specified along the solid boundary $\xi_1 = 0$, the value of σ_1 in the left state, σ_{1L}, based on the boundary value σ_{1b} has the form

$$\sigma_{1L} = \sigma_{1b}\frac{q_L^*}{q_L}. \tag{18}$$

For the other RPs, σ_1 in the right state, σ_{1R}, is used to calculate σ_1 in the centred state, $\sigma_1{}^*$, and in the left state, σ_{1L}, as

$$\sigma_1^* = \sigma_{1R}\frac{q_R}{q_R^*}, \qquad \sigma_{1L} = \sigma_{1R}\frac{q_L^*}{q_L}\frac{q_R}{q_R^*}. \tag{19}$$

For σ_{1b} specified along the far-field boundary $\xi_2 = 1$, the value of σ_1 in the right state, σ_{1R}, based on the boundary value σ_{1b} has the form

$$\sigma_{1R} = \sigma_{1b}\frac{q_R^*}{q_R}. \tag{20}$$

For the other RPs, σ_1 in the left state, σ_{1L}, is used to calculate σ_1 in the centred state, σ_1^*, and in the right state, σ_{1R}, as

$$\sigma_1^* = \sigma_{1L}\frac{q_L}{q_L^*}, \qquad \sigma_{1R} = \sigma_{1L}\frac{q_L}{q_L^*}\frac{q_R^*}{q_R}. \tag{21}$$

For rarefaction waves the positions (see Figure 5) of the leading and trailing Mach waves for the streamwise increment $\Delta\xi_1$ are determined from

$$\Omega_{L,R} = \pm\frac{(\sigma_1)_{L,R}\Delta\xi_1}{(\sigma_2)_{L,R}\Delta\xi_2}\tan(\mu_{L,R}), \tag{22a}$$

$$\Omega_{L,R}^{*} = \pm\frac{\sigma_1^{*}}{(\sigma_2^{*})_{L,R}}\frac{\Delta\xi_1}{\Delta\xi_2}\tan(\mu_{L,R}^{*}), \tag{22b}$$

where $\Omega_{L,R}, \Omega_{L,R}^{*} \in [-\frac{1}{2}, \frac{1}{2}]$ are fractions of $\Delta\xi_2$ with respect to the position of the initial discontinuity $(\xi_2)_{j-1/2}$. For oblique shock waves the positions are determined from

$$\Omega_{L,R} = \frac{(\sigma_1)_{L,R}\Delta\xi_1}{(\sigma_2)_{L,R}\Delta\xi_2}\tan(\beta_{L,R}), \tag{23}$$

since $\Omega_{L,R} = \Omega_{L,R}^{*} \in [-\frac{1}{2}, \frac{1}{2}]$.

Considering the jth cell in isolation, waves propagate outwards from the interfaces with the CFL condition stopping them from interacting with each other. To calculate the vector of primitive variables (except σ_1) downstream at the new spatial point, $\bar{U}_{i+1,j}$, the interval $(\xi_2)_{j-1/2} \leqslant \xi_2 \leqslant (\xi_2)_{j+1/2}$ is sampled randomly (see Figure 6) with the sampling point P_{i+1} defined by the co-ordinates $\{(\xi_1)_{i+1}, (\xi_2)_{j-1/2} + \Omega_{i+1}\Delta\xi_2\}$. Following Colella,[3] we use the Van der Corput equidistributed pseudorandom number series to generate $\Omega_{i+1} \in [0, 1]$. The solution $\bar{U}_{i+1,j}$ is determined by the calculated conditions at the sampling point.

For $0 \leqslant \Omega_{i+1} < \frac{1}{2}$ the RP$(j-1, j)$ is solved with sampling in the top quadrant. Wave angles are measured with respect to the streamline position $(\xi_2)_{j-1/2}$ and are positive. For rarefaction waves, $\Omega_{i+1} > \Omega_L \Rightarrow \bar{U}_{i+1,j} = \bar{U}_L$ and $\Omega_{i+1} < \Omega_L^{*} \Rightarrow \bar{U}_{i+1,j} = \bar{U}_L^{*}$. For $\Omega_L^{*} < \Omega_{i+1} < \Omega_L$ the primitive variables are determined by solving the characteristic wave equation in (s, n) space for pressure,

$$\Omega_{i+1}\frac{\sigma_2\Delta\xi_2}{\sigma_1\Delta\xi_1} = \tan(\mu), \tag{24}$$

where

$$\frac{\sigma_2}{\sigma_1} = \eta^{-1/\gamma}\frac{\sigma_{2L}}{\sigma_{1L}}, \qquad M = \sqrt{\left\{\frac{2}{\gamma-1}\left[(\eta^{(1-\gamma)/\gamma}\left(1+\frac{\gamma-1}{2}M_L^2\right)-1\right]\right\}} \tag{25}$$

and $\eta = p/p_L$. For oblique shock waves, $\Omega_{i+1} > \Omega_L \Rightarrow \bar{U}_{i+1,j} = \bar{U}_L$ and $\Omega_{i+1} < \Omega_L \Rightarrow \bar{U}_{i+1,j} = \bar{U}_L^{*}$.

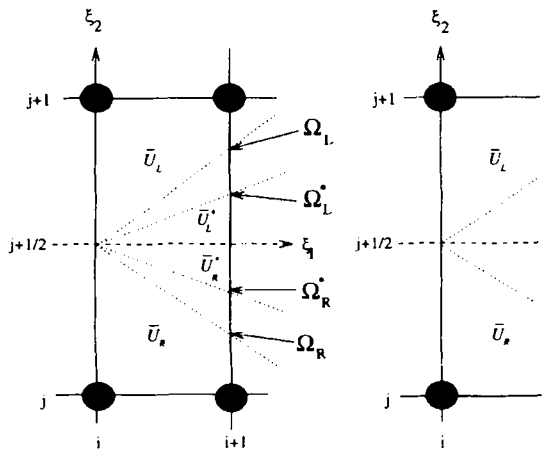

Figure 5. Wave positions in Riemann problem

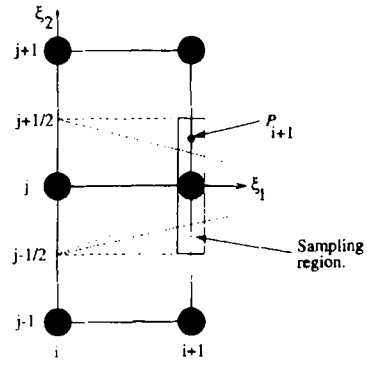

Figure 6. Sampling region

For $\frac{1}{2} < \Omega_{i+1} \leqslant 1$ the RP$(j, j+1)$ is solved with sampling in the bottom quadrant. Wave angles are measured with respect to the streamline position $(\xi_2)_{j+1/2}$ and are negative. For rarefaction waves, $\Omega_{i+1} - 1 < \Omega_R \Rightarrow \bar{U}_{i+1,j} = \bar{U}_R$ and $\Omega_{i+1} - 1 > \Omega_R^* \Rightarrow \bar{U}_{i+1,j} = \bar{U}_R^*$. For $\Omega_R < \Omega_{i+1} - 1 < \Omega_R^*$ the primitive variables are determined by solving the characteristic wave equation in (s, n) space for pressure,

$$(\Omega_{i+1} - 1)\frac{\sigma_2 \Delta\xi_2}{\sigma_1 \Delta\xi_1} = -\tan(\mu), \tag{26}$$

where

$$\frac{\sigma_2}{\sigma_1} = \eta^{1/\gamma}\frac{\sigma_{2R}}{\sigma_{1R}}, \qquad M = \sqrt{\left\{\frac{2}{\gamma - 1}\left[\eta(1-\gamma)/\gamma\left(1 + \frac{\gamma - 1}{2}M_R^2\right) - 1\right]\right\}} \tag{27}$$

and $\eta = p/p_R$. For oblique shock waves, $\Omega_{i+1} - 1 < \Omega_R \Rightarrow \bar{U}_{i+1,j} = \bar{U}_R$ and $\Omega_{i+1} - 1 > \Omega_R \Rightarrow \bar{U}_{i+1,j} = \bar{U}_R^*$.

Once the numerical solution in (ξ_1, ξ_2) space has been determined, the system (5a, b) can be used to transform it to Cartesian space (x_1, x_2).

4. RESULTS AND DISCUSSION

In Figure 7 we have computed the flow of $M = 2$ past an expression angle of 10° which produces a PM rarefaction wave; 100 cells were used in the computation. The numerical wave positions and variations in pressure and density ratios through the fan for the streamline $\xi_2 = 0{\cdot}115$ are in excellent agreement with the analytical solution. In Figure 8 the expansion angle was increased to 30°. The computed wave positions and variations in pressure and density ratios through the fan for the streamline $\xi_2 = 0{\cdot}045$ are again in excellent agreement.

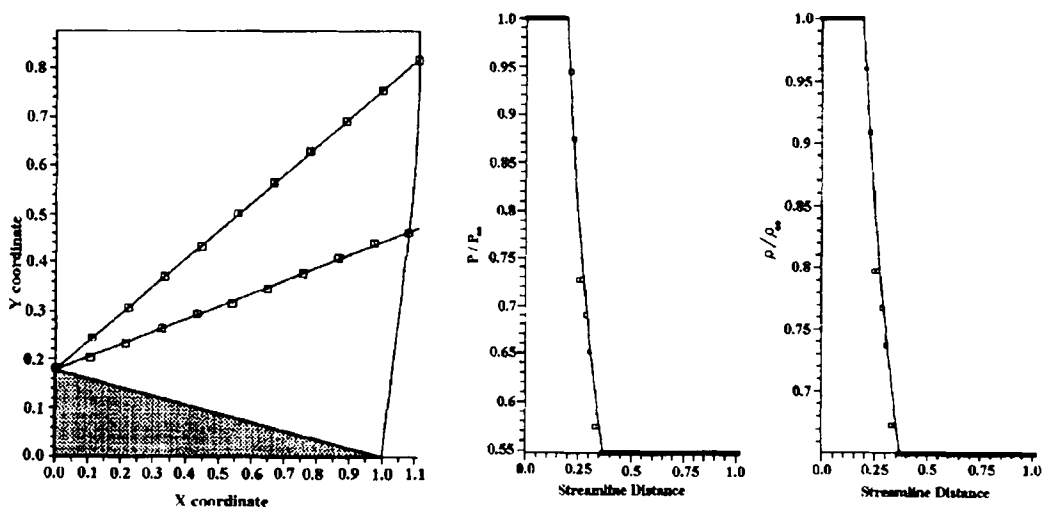

Figure 7. Comparison between analytic (line) and numerical (symbol) solutions for PM rarefaction wave. $M = 2, \theta_W = -10°$

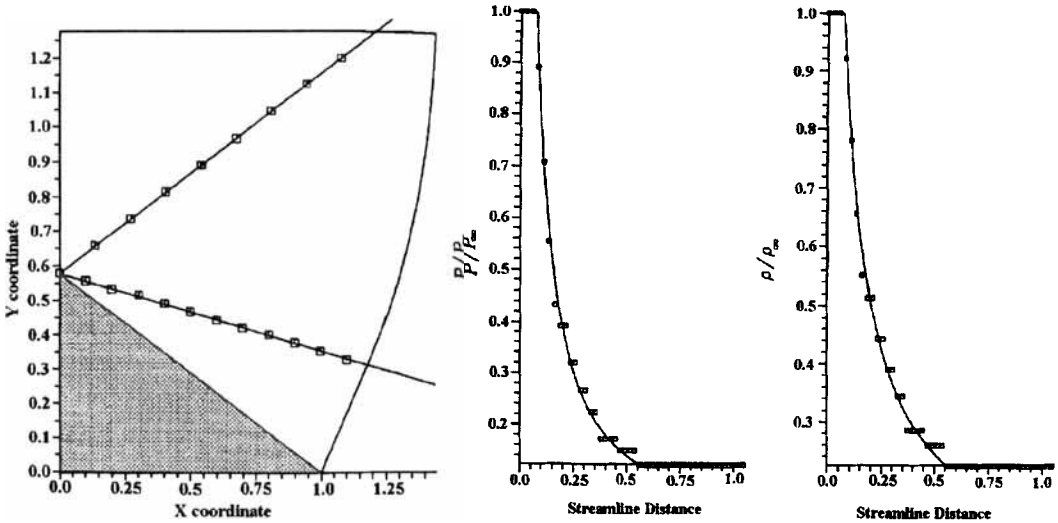

Figure 8. Comparison between analytic (line) and numerical (symbol) solutions for PM rarefaction wave. $M = 2$, $\theta_W = -30°$

The flow past a wedge with a sharp compressive angle of 30° was computed, using 100 cells, for four different Mach numbers in Figure 9. Even after the computed flow field has been transformed from (ξ_1, ξ_2) to Cartesian space (x, y), the numerical wave positions are excellent.

The flow of $M = 7{\cdot}4$ past a double wedge with leading and trailing flow deflection angles of $\theta_1 = 8°$ and $\theta_2 = 19°$ respectively was computed. The flow deflections produce two oblique shock waves which collide. At this point an oblique shock wave, contact wave and secondary wave

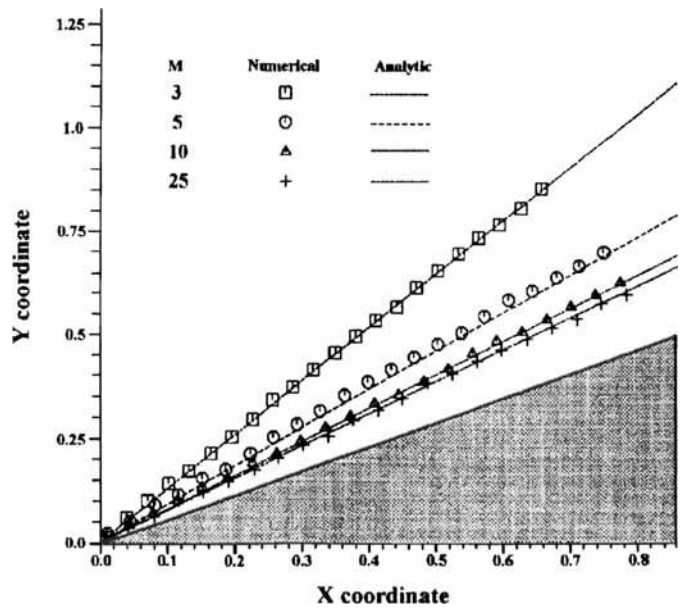

Figure 9. Comparison between analytic (line) and numerical (symbol) oblique shock wave positions for upersonic flow over a 30° wedge

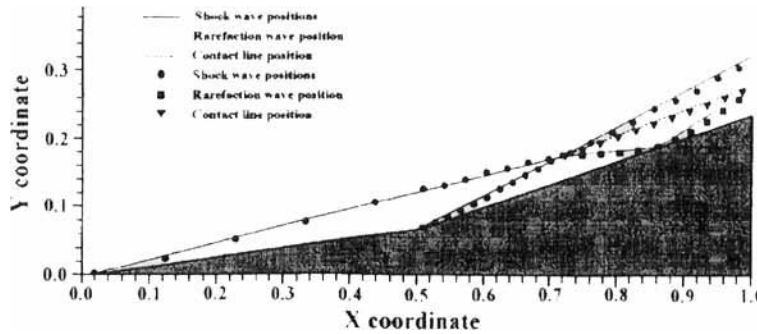

Figure 10. Comparison between analytic (lines) and numerical (symbols) wave positions for supersonic flow over a double wedge. $M = 7{\cdot}4, \theta_1 = 8°, \theta_2 = 19°$

(rarefaction of shock) are generated. The strength and type of the latter are determined from the intersection of the shock polars[22] for the shock waves before collision together with the constraint that the pressure is constant across the contact. For the prescribed conditions the secondary wave is a rarefaction. The computed (100 cells) and analytic wave positions are presented in Figure 10 with good agreement between the two.

The flow field past a half-diamond configuration with deflection angles $\theta_1 = 10°$ and $\theta_2 = -10°$ for $M = 5$ (see Figure 11) and $M = 15$ (see Figure 12) was computed using 1500 cells. The interaction of the incident (rarefaction) wave with the leading shock wave weakens it, with secondary (reflected) waves (rarefaction or shock) being generated.[23] These travel downwards, away from the point of interaction. A reflection coefficient[23,24] R_v based on the ratio of the pressure difference across the reflected and incident waves can be defined. For positive values the reflected and incident waves are of the same type. For negative R_v the reflected wave type is opposite to the incident wave. The variation in R_v with flow deflection angle for $\gamma = 1{\cdot}4$ has been calculated for several different Mach numbers and is presented in Figure 13. For the initial flow deflection θ_1 it is observed the R_v is negative for both flow conditions. The analytic position of the leading shock wave was calculated

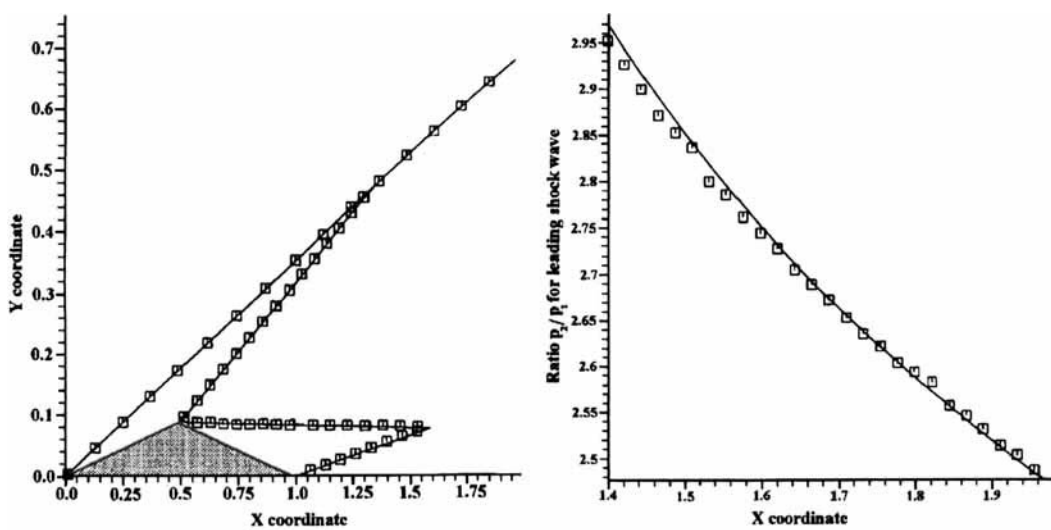

Figure 11. Half-diamond configuration. $\theta_1 = 10°, \theta_2 = -10°, M = 5$

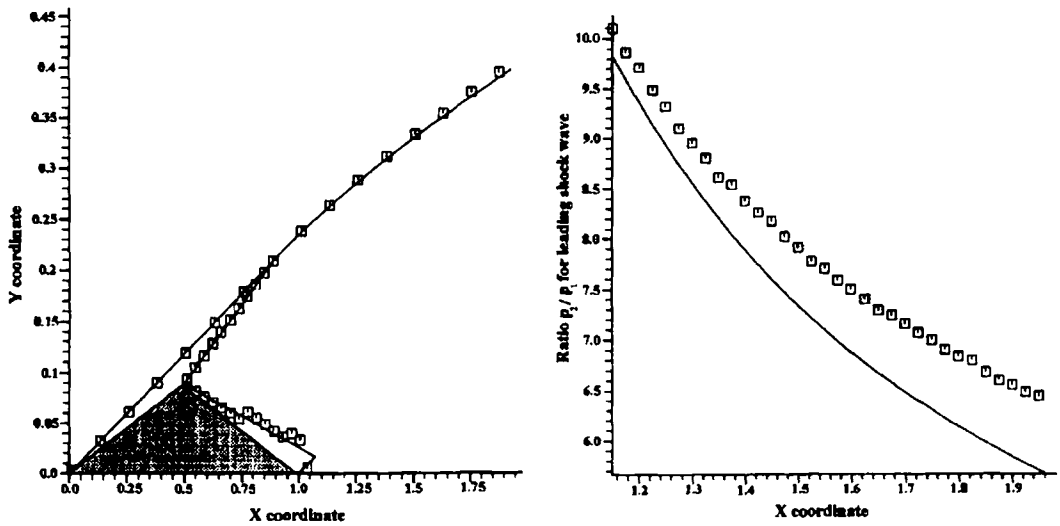

Figure 12. Half-diamond configuration. $\theta_1 = 10\,\text{deg}, \theta_2 = -10\,\text{deg}, M = 15$

using shock expansion (SE) theory,[23] which assumes that the reflected wave strengths are negligible compared with the incident wave strength. For $M = 5$ the analytic and numerical leading shock wave positions and pressure ratios are very nearly coincident. This is because the magnitude of R_v is very small and SE theory is a good approximation in this instance. For $M = 15$ the magnitude of R_v is much larger. Therefore the discrepancies between the analytic and numerical leading shock wave positions and pressure ratios are as expected, since SE theory is no longer applicable.

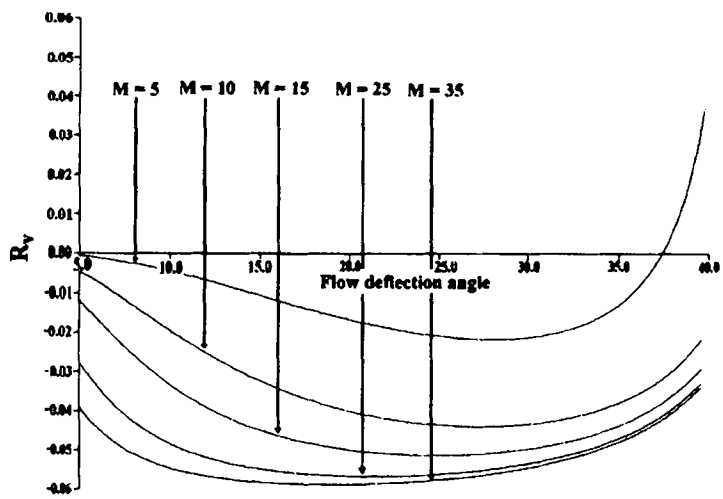

Figure 13. Calculated reflection coefficeints R_v for $\gamma = 1{\cdot}4$

5. CONCLUDING REMARKS

Glimm's random choice method for natural co-ordinates has been successfully applied to several different configurations. Computed results have shown a good accuracy, with wave positions captured crisply and with no numerical smearing. Complex boundaries are treated with ease, with no special procedures necessary.

ACKNOWLEDGEMENTS

I wish to thank J. F. Clarke F.R.S., Emeritus Professor of Theoretical Gas Dynamics, Cranfield University, Bedford, U.K. for all his time and help during this work.

REFERENCES

1. J. Glimm, 'Solutions in the large for nonlinear hyperbolic systems of equations', *Commun. Pure Appl. Maths.*, **XVIII**, 697–715 (1965).
2. A. J. Chorin, 'Random choice solution of hyperbolic systems', *J. Comput. Phys.*, **22**, 517–533 (1976).
3. P. Colella, 'Glimms's method for gas dynamics', *SIAM J. Sci. Stat. Comput.*, **3**, 76–110 (1982).
4. J. J. Gottlieb, 'Staggered and nonstaggered grids with variable node spacing and local time stepping for the random choice method', *J. Comput. Phys.*, **78**, 160–177 (1988).
5. G. A. Sod, 'A numerical study of a converging cylindrical shock,' *J. Fliud Mech.*, **83**, 785–794 (1977).
6. E. F. Toro, 'The random choice method on a nonstaggered grid utilising an efficient riemann solver *College of Aeronautics, Cranfield, Tech. Rep. 8708*, 1987.
7. H. Honma, M. Wada and K. Inomata, 'Random choice method for two dimensional and axisymmetrical supersonic flows', *Insitute of Space and Astronautical Science Rep. S.P. No. 2*, 1984.
8. G. Marshall and B. Plohr, 'A random choice method for two dimensional steady supersonic shock wave diffraction problems', *J. Comput. Phys.*, **56**, 410–427 (1984).
9. H. Oliver and H. Grönig, 'The random choice method applied to two dimensional shock focusing and diffraction', *J. Comput. Phys.* **63**, 85–106 (1986).
10. Z. C. Shi and J. J. Gottlieb, 'Random choice method for two dimensional planar and axisymmetric steady supersonic flows,' *UTIAS Rep. 297*, 1985.
11. C. Y. Loh and W. H. Hui, 'A new lagrangian random choice method for steady two dimensional supersonic/hypersonic flow', *AIAA Paper 91-1546-CP*, 1991.
12. C. Hirsch, *Numerical Computation of Internal and External Flows*, Vol. 1, Wiley, Chichester, 1988.
13. C. Hirsch, *Numerical Computation of Internal and External Flows*, Vol. 2, Wiley, Chichester, 1990.
14. E. F. Toro, 'Random choice based hybrid methods for one and two dimensional gas dynamics', *College of Aeronautics, Cranfield, Tech. Rep. 8801*, 1988.
15. M. R. Spiegal, *Vector Analysis*, McGraw-Hill, New York, 1959.
16. M. Vinokur, 'Conservation equations of gas dynamics in curvilinear coordinate systems', *J. Comput. Phys.*, **14**, 105–125 (1974).
17. G. Emanuel, *Gas Dynamics: Theory and Applications*, AIAA, New York, 1986.
18. A. S. Dawes, 'Natural coordinates and high speed flows. A numerical method for reactive gases *Ph.D. Thesis*, College of Aeronautics, Cranfield, 1992.
19. J. D. Anderson Jr., *Modern Compressible Flow with Historical Perspective*, McGraw–Hill, New York, 1982.
20. R. Courant, K. O. Friedrichs and H. Lewy, 'On the partial difference equations for mathematical physics,' *IBM J.*, March, (1967) (English translation).
21. C. Fröberg, *Introduction to Numerical Analysis*, 2nd edn, Addision-Wesley, Reading, MA, 1969.
22. R. Courant and K. O. Friedrichs, *Supersonic Flow and Shock Waves*, Interscience, New York, 1948.
23. W. D. Hayes and R. F. Probstein, *Hypersonic Flow Theory*, Vol. 1, 2nd edn, Academic, New York, 1966.
24. A. J. Eggers Jr., C. A. Syvertson and S. Kraus, 'A study of inviscid flow about airfoils at high supersonic speeds', *NACA Rep. 1123*, 1953.